The role of beam dispersion in Raman and photo-stimulated luminescence piezo-spectroscopy of yttria-stabilized zirconia in multi-layered coatings

Dong Liu[a, b,],
Oliver Lord[c, 1],
Oliver Stevens[a],
Peter E.J. Flewitt[a, d]

doi:10.1016/j.actamat.2012.08.052

Abstract

Laser beam dispersion affects the resolution of Raman and photo-stimulated luminescence piezo-spectroscopy measurements of transparent materials. In this paper, we investigate the lateral spreading of the laser beam and the axial sampling depth of Raman spectroscopy measurements within thermal sprayed yttria-stabilized zirconia (YSZ) thin coatings. The lateral diameters of the laser beams (λ = 632.8 nm and 514 nm) reach approximately ~160 μm after travelling through a thickness of 200 μm of air plasma sprayed (APS) YSZ and ~80 μm after travelling through 120 μm of electron beam physical vapour deposited YSZ. The Raman spectroscopy sampling depth was found to be between 30 and 40 μm in APS YSZ. The beam dispersions within these two coatings were simulated using the ray-tracing software ZEMAX to understand the observed scattering patterns. The results are discussed with respect to the application of these two spectroscopic techniques in multi-layered thermal barrier coating systems.

Keywords

Yttria-stabilized zirconia ceramics;
Raman spectroscopy;
Fluorescence;
Plasma spray coatings;
Modelling

1. Introduction

Zirconia thin films have been extensively investigated due to their numerous applications and superior properties: low thermal conductivity, high dielectric constant, high optical refractive index, chemical durability, mechanical strength and fracture toughness [1]. One of the most important applications for zirconia thin films is as a thermal barrier coating (TBC) for components working at high temperatures. Typically, a thin layer (~200–300 μm) of yttria-stabilized tetragonal zirconia (YSZ) is applied to the blades of high-pressure

turbines of land-based power generators. The thickness varies with position on the blade surface. The low thermal conductivity of the layer allows coated components to operate at higher temperatures than the underlying parent metal can withstand. Therefore it is crucial for the layers to remain attached to the components and to be tolerant to the residual stresses and thermal cycling encountered during service[2] and [3]. These thermal barrier coatings (TBCs) comprise a multi-layer consisting of a top layer of YSZ, a metallic bond coat (BC) that provides bonding between the metallic substrate and YSZ and finally a thermally grown oxide (TGO) layer that forms between the TBC and BC during thermal exposure [4]. The growth of this oxide [3] and the sintering [5] of the YSZ layer during thermal ageing are the main sources of residual stresses in the TGO and YSZ and lead to the eventual failure of the coating system. The extensive use of the YSZ layer as a TBC has given rise to much research focused on how the degradation of this coating system depends upon different application methods [6], the microstructure of the coatings [7] and [8], and the residual stress distributions in the YSZ and TGO layers [9], [10] and [11].

Among the non-destructive approaches to material investigation, Raman and photo-stimulated luminescence piezeo-spectroscopy (PLPS) are the techniques favoured for the measurement of stresses in YSZ and TGO respectively. The peaks in the Raman spectra associated with the YSZ shift as a function of local strain. These peak shifts can be calibrated so that Raman spectra can be used to calculate the stress in the coating[12], [13] and [14]. However, zirconia-based ceramic coatings are translucent because the optical band gap for these materials is ~12 eV, which is well above the energy of the argon-ion and He–Ne lasers (λ = 514 nm and λ = 632.8 nm) and the characteristic ruby-fluorescence doublet of a-Al_2O_3 at 694.3 nm and 693 nm [15]. Unfortunately, the complex microstructure of the applied translucent material reduces the resolution of the measurements dramatically due to dispersion [16]. The assumption generally made for stress measurements on air plasma sprayed APS-YSZ is that the Raman signal acquired is limited to the near surface but without specifying the range of depth [17]. Recent experimental studies have shown that the sampling depth can reach 20–50 μm even in dense YSZ [18]. As sampling depth increases the resolution decreases due to beam dispersion. This dispersion is a consequence of internal boundaries, pores and other imperfections within both APS-YSZ and electron beam physical vapour deposited EBPVD-YSZ.

The sampling depth for Raman spectroscopy depends upon the specific microstructure and optical properties of the material. Higher-resolution measurements can be expected for more opaque materials such as silicon [19] and [20] or when using ultraviolet laser radiation [20]. Even though the depth resolution can be improved by the use of a confocal Raman system combined with oil-immersed objective lenses [21] and [22], the depth resolution in translucent materials can be reduced significantly due to refraction [23] and spherical aberration [24] of the light in the part of the laser beam path within the out-of-focus area [25].

The lateral spreading of the laser beam is directly related to the spatial resolution for measurements. In bulk material, the size of the cone-like excitation volume depends on the numerical aperture of the objective lens and the difference in refractive index between the material in which the objective is immersed and the material being investigated [18], [23] and [26]. For materials with porous microstructures, such as thermally sprayed YSZ, the lateral resolution can be further reduced by the scattering of the laser beam by pores and unmelted particles [27] and by ray guiding [28] when the incident beam strikes the internal splat boundaries at an angle greater than the critical refraction angle [29]. This dispersion of the beam has to be established experimentally because there are too many unquantified variables within the overall microstructure [30](Fig. 1a and b) to allow realistic, quantitative theoretical calculations to be made.

Fig. 1.

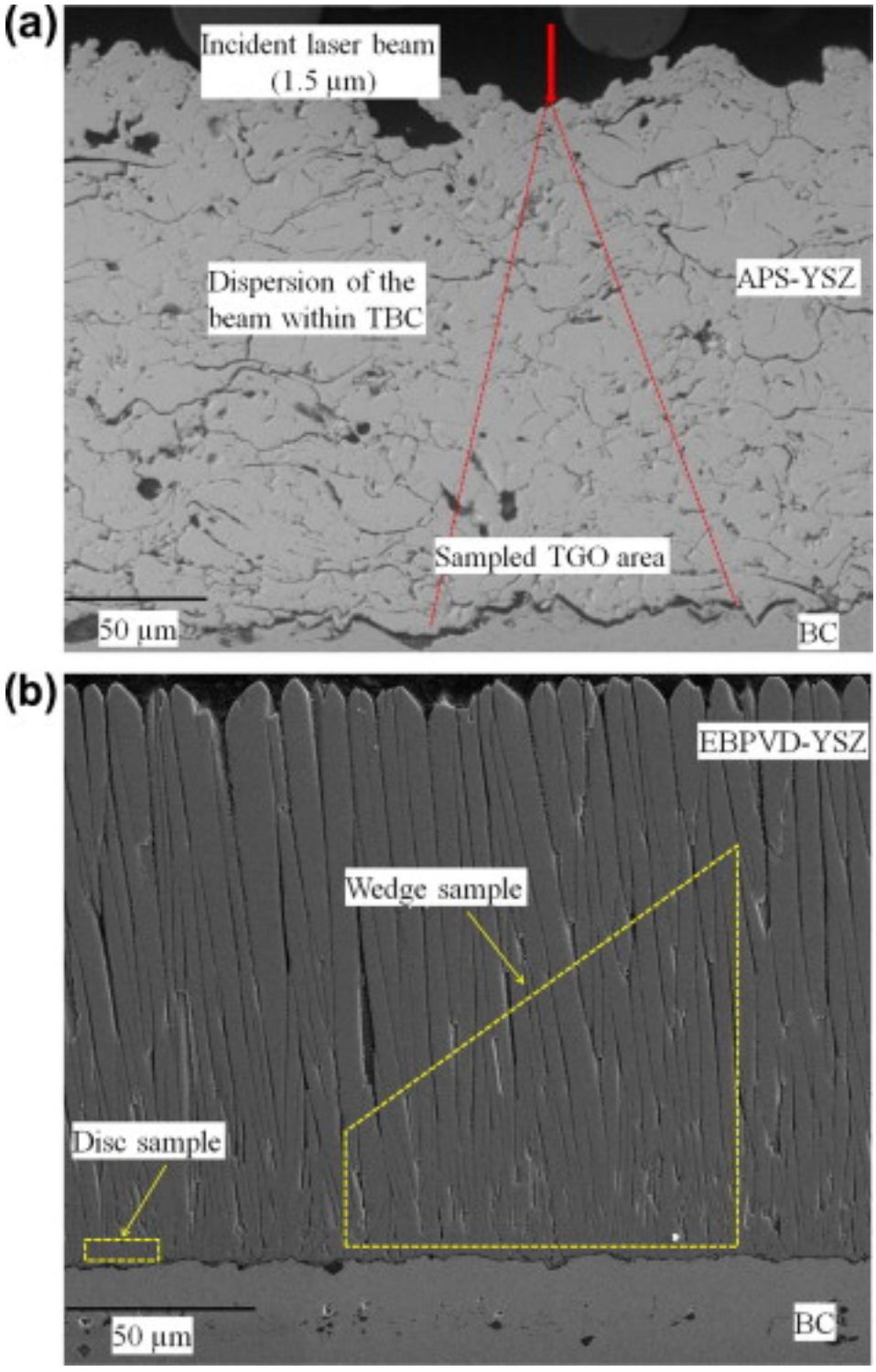

Secondary electron images of the microstructure of (a) APS-YSZ and (b) EBPVD-YSZ.

Since the TGO develops at the interface between the BC and the TBC, it is buried below the coating layer. The TGO layer is mainly α-Al_2O_3 doped with chromium ions (Cr^{3+}) which produce the characteristic luminescence R1 and R2 lines (λ = 693 and 694.3 nm) when stimulated with the laser light used for PLPS [31]. The positions of these lines change with stress and have been calibrated on a ruby standard by Clarke et al.[10] and [32] allowing PLPS to be used for the measurement of stress in various alumina-containing materials [33] and [34]. As a consequence, when undertaking PLPS measurements of stresses within the TGO, lateral spreading of the incident laser beam within the TBC will affect the measurement resolution, which is defined by the diameter of the laser at the TGO surface [35]. This resolution is important, for example, for defining the step size when mapping stress in the TGO through the YSZ layer to avoid overlap of the measurements and thereby provide more reliable stress information [36],[37] and [38].
In this paper, the laser beam spreading and the sampling depth of Raman spectroscopy within the YSZ is investigated. For practical purposes, two types of YSZ coatings that are widely used in industry were selected.

2. Experimental

Two YSZ (7 wt.% yttria-stabilized tetragonal zirconia) commercial TBC materials have been considered: (i) APS and (ii) EBPVD. The APS-YSZ forms a coating consisting of micro-scale multilayers of overlapping thin lenticular particles, or splats (Fig. 1a), whereas the EBPVD-YSZ possesses a columnar microstructure (Fig. 1b), which has higher lateral strain tolerance and higher thermal conductivity [27]. Raman spectroscopic measurements were made using a Renishaw Ramascope model 2000 spectrometer, fitted with both Ar and He–Ne laser sources operating at wavelengths of 514 nm (30 mW) and 632.8 nm (25 mW) respectively. Both Raman spectroscopy and PLPS measurements can be made using this system. A long working distance (LWD) Olympus lens with a 50 × magnification and a numerical aperture of 0.55 was used.
The BC of the two types of specimens, APS-YSZ and EBPVD-YSZ, are both ~50 μm thick flat NiCoCrAlY (Fig. 1). Tapered wedge specimens (see Fig. 1a) were cut using UV laser ablation from both the as-sprayed APS-YSZ samples (with thickness varying from 8 to 200 μm) and the as-deposited EBPVD-YSZ sample (with thickness varying from 60 to 120 μm). In addition, two thin discs were prepared from the EBPVD material with thicknesses of ~5 and ~19 μm and both ~100 μm in diameter (see Fig. 1b). The incident laser beams used were focused to a 1.5 μm beam diameter. An adjustable digital microscopy camera with a pixel resolution of 1280 × 960 (1.3 million pixels) was positioned below the specimen to monitor the dispersed laser beam (Fig. 2a). The images were transferred to Mica software and analysed using intensity line-scanning. A typical laser intensity profile is shown in Fig. 2b, where the beam diameter is defined by the full width at half maximum (FWHM).

Fig. 2.

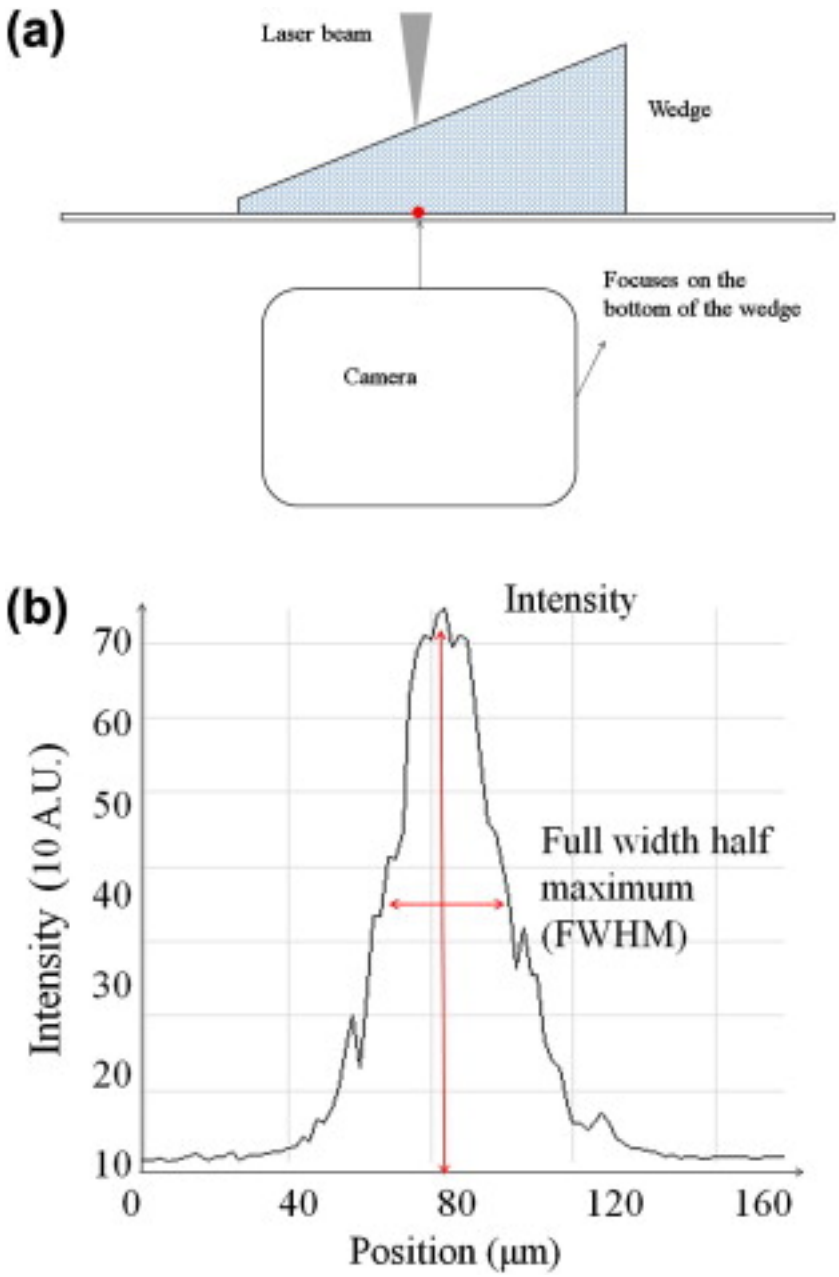

(a) Schematic of experimental set-up and (b) a typical laser intensity profile and the definition of the beam diameter.

In addition, one of the as-sprayed APS-YSZ samples was heat treated at 925 °C for 100 h in air to allow the Al to diffuse from the NiCoCrAlY-BC, forming a dense TGO layer of α-alumina between the YSZ and the NiCoCrAlY-BC. Again, a tapered wedge of this sample was prepared using UV laser ablation with a thickness which varied from 10 to 250 μm. The signal of YSZ and the underlying alumina were collected from the top surface of the YSZ layer as before. To investigate the depth of the Raman signal collected, line scans were made across the wedged samples and the intensity of the Raman spectra for the YSZ and the TGO layer measured at regular intervals.

3. Modelling

To better understand and visualize the behaviour of light propagation though the APS-YSZ and EBPVD-YSZ materials, optical ray-tracing models were created based upon simplified microstructures. A ray-tracing software package (ZEMAX, ZEMAX Corporation) was used to simulate illumination of the samples with a 632.8 nm wavelength laser. For all ray-tracing experiments ZEMAX was operated in the “non-sequential” mode, which performs a Monte Carlo simulation in which each ray is not limited to forward progression through the optical system and can pass in any direction. In each simulation, 10^5 rays were traced, and the results were measured from a plane at the bottom of the YSZ. The laser illumination system was simulated using a monochromatic, λ = 632.8 nm, a Gaussian source and a numerical aperture 0.55, with a 1.5 μm diameter incident beam spot diameter (FWHM) at the sample surface. YSZ was simulated using a material of refractive index 2.

4. Results

The experimental results are addressed in Sections 4.1 (laser beam dispersion) and 4.2 (sampling depth). The modelling results presented in Section 4.3 provide an aid to understand the laser beam dispersion behaviour within the simplified representative model.

4.1. Experimental

4.1.1. Laser beam dispersion

The variation of measured beam diameter with the thickness of the APS-YSZ is shown inFig. 3 for the two laser wavelengths, red and green, used (λ = 514 nm and λ = 632.8 nm). The standard deviations of the data were calculated from three measurements undertaken for each thickness. The error in the thickness measurement is a fixed value of ±2 μm shown in the figures by the size of the symbols. As shown in Fig. 3, the diameter, D(μm), of the red and green laser beams increased monotonically with APS-YSZ thickness, t (μm), from zero to 200 μm. The data were best fitted by an exponential function:

equation(1)

$$D = D_0 + a \cdot \exp(-t/b),$$

where D_0 = 194.00 μm, a = −192.50 and b = 97.65 are constants and give a fit with a statistic fit index R^2 value of 0.98 for the green laser beam,
and D_0 = 177.20 μm,a = −175.70 and b = 51.33 give a fit with a R^2 value of 0.99 for the red laser beam. Since there is scatter in the measured diameters and all data lie within these bands, it is appropriate to consider a single fit to all the data. The resulting curve (Fig. 3), has aR^2 value of 0.97, where D_0 = 182.73 μm, a = −181.23, b = 76.22.

Fig. 3.

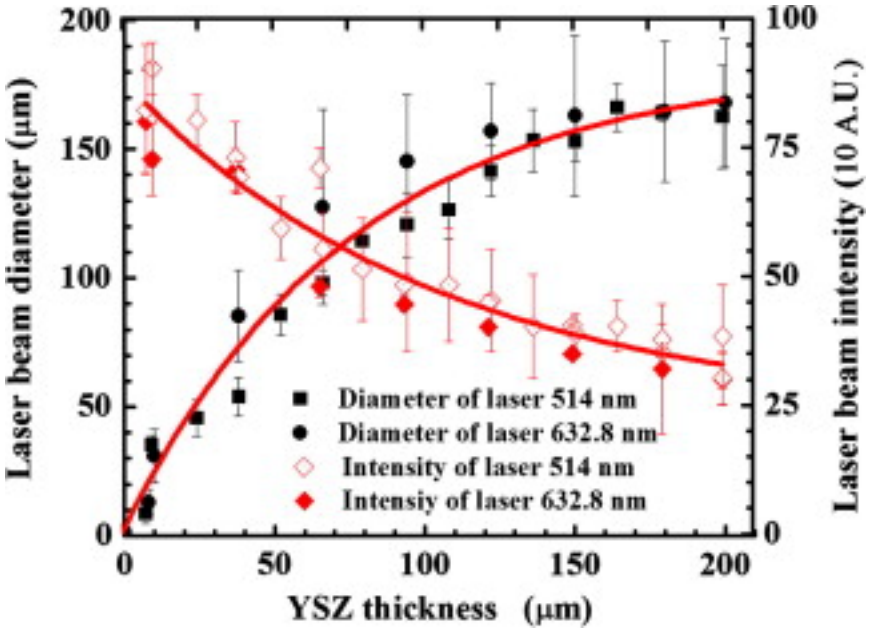

The variation of red (λ = 632.8 nm) and green laser (λ = 514 nm) beam diameters with APS-YSZ thickness.

As the laser beam is increasingly dispersed, the intensity, I, decays. Fig. 3 shows that this follows an exponential decay with increasing APS-YSZ thickness, t (μm), given by:

equation(2)

$$I = I_0 + A \cdot \exp(-t/B),$$

where I_0 is the initial intensity, A and B are constants, and t is the thickness of the APS-YSZ. In this specific type of APS-YSZ, I_0 = 22.97, A = 64.94, B = 104.83, the index R^2 = 0.94 confirms high confidence in the fitted curve to these data.
Fig. 4 shows the variation in laser beam diameter with thickness, t (μm), for the two EBPVD-YSZ wedges. Measurements using red and green lasers were made at three points for each TBC thickness. Both of these data sets, as well as values determined from the ~5 and ~19 μm thick discs are consistent, which indicates an adequate repeatability of this experimental approach regardless of variations in microstructure. Both the scattered diameters for green and red lasers, D (μm), increase exponentially with the thickness, t (μm), and reach ~80 μm at a thickness of 120 μm, following Eq. (1)with

constants of D_0 = 80.30, a = −79.80, b = 37.04 and R^2 = 0.96 for the green laser andD_0 = 81.43, a = −79.93, b = 34.04 and R^2 = 0.94 for the red laser. Since the two groups of data overlap, the data were combined, yielding a fit with D_0 = 83.14, a = −81.64, b = 40.69 and R^2 = 0.96. The intensity decay from one of the wedges is shown in Fig. 4, following Eq. (2) with I_0 = 22.93, A = 72.04 and B = 79.47.

Fig. 4.

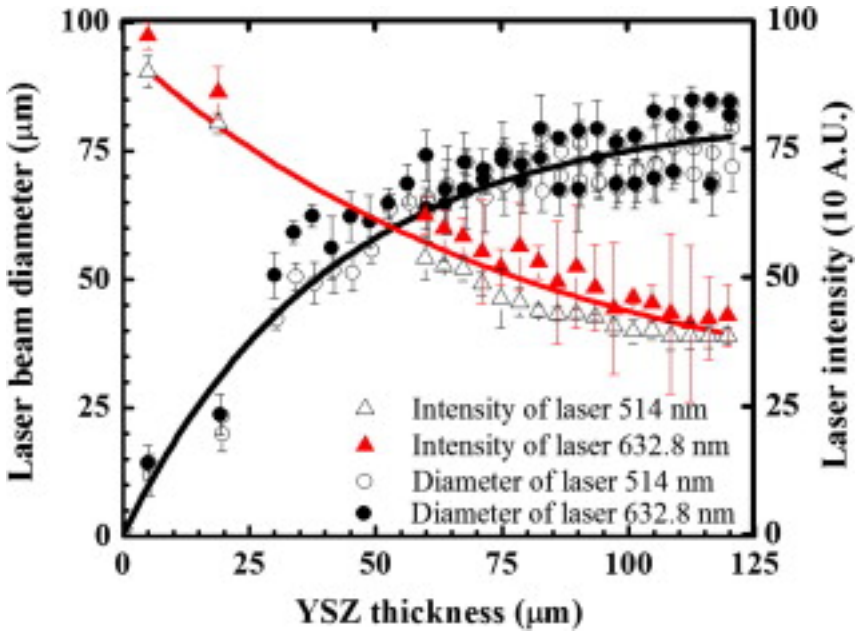

The variation of red (λ = 632.8 nm) and green laser (λ = 514 nm) beam diameters with EBPVD-YSZ thickness.

4.1.2. Sampling depth

The schematic diagram shown in Fig. 5a summarizes the basis of the experiment undertaken to evaluate the depth of material sampled by the incident laser beam during Raman spectroscopy. The APS-YSZ wedge sample has a thickness of ~10 μm at one end and ~250 μm at the other, with a uniform layer of α-alumina below. Raman spectra were collected at each thickness as the laser beam was moved along the APS-YSZ wedge in the direction of increasing thickness (positions 1–4 in Fig. 5a). In Fig. 5b, three spectra of the YSZ and α-alumina collected at thicknesses of 50, 100 and 180 μm covering both the Raman and PLPS measurement range are vertically displaced to show the significant drop in intensity for the α-alumina peaks (5023 and 5053 cm^{-1}) with the increasing thickness of the YSZ layer.

Fig. 5.

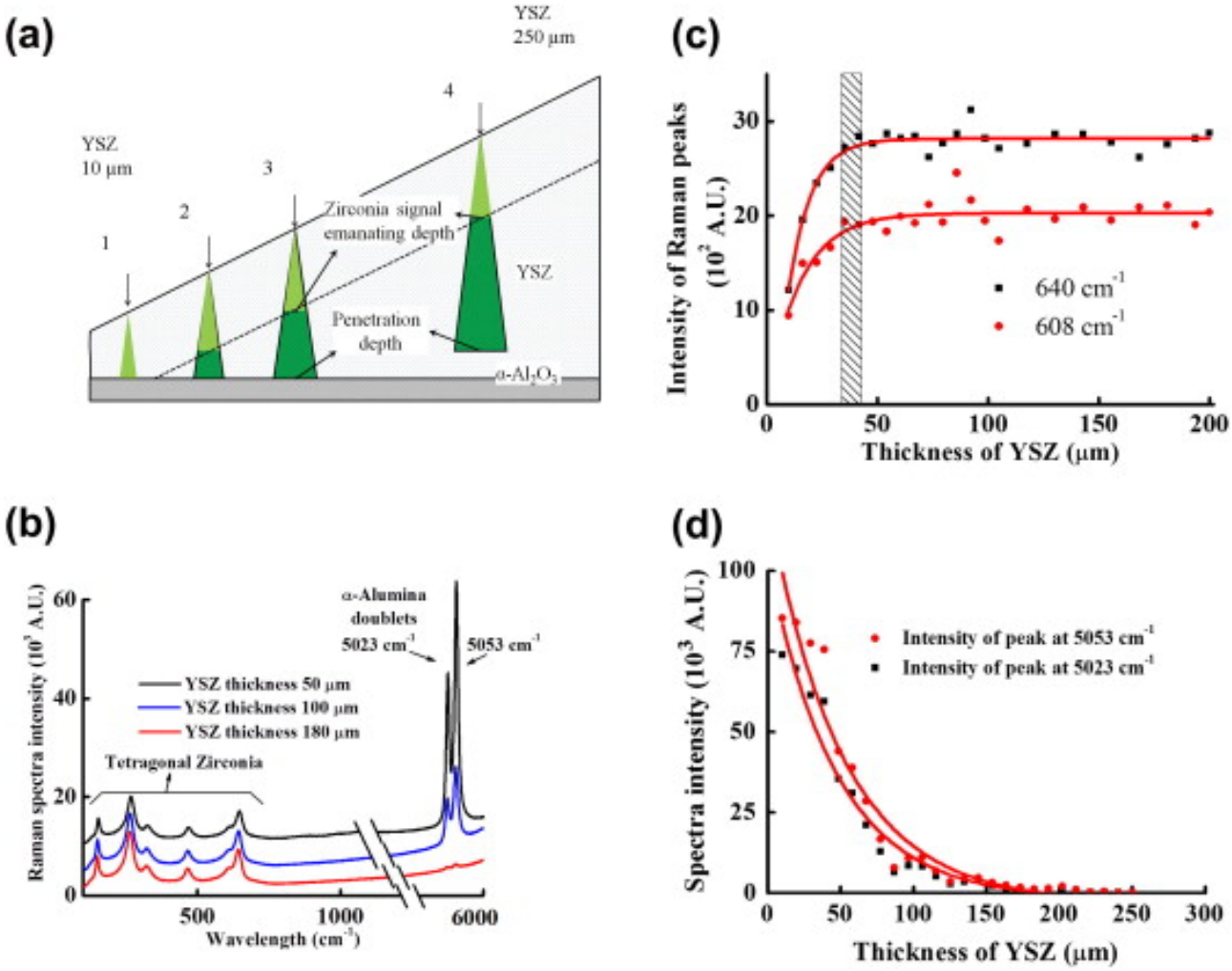

(a) The schematic of the set-up for the measurements of intensity of the Raman spectra of a wedged APS-YSZ/α-alumina sample; (b) Raman spectra for YSZ and α-alumina; (c) the exponential increase of the intensities of two Raman peaks with YSZ thickness. A stable platform is achieved when the thickness is larger than 40 μm, with an error in thickness of about 5 μm. (d) The decrease in the α-alumina doublet intensity with the increase in the YSZ layer thickness.

There are six peaks for the Raman spectrum of YSZ. Each spectrum was fitted using mixed Gaussian and Lorentzian equations [39]. The peaks centred at 608 and 640 cm^{-1}were chosen for investigation because of their large signal-to-noise ratio, and the intensity recorded at each YSZ thickness. As shown in Fig. 5c, the Raman peak intensities of 608 and 640 cm^{-1} both increase exponentially as the thickness of the YSZ coating increases until this reaches about 40 ± 2 μm. The intensity then remains relatively stable up to the limit of the measurements. This is consistent when moving progressively from position 1 to positions 2–4 in Fig. 5b and defines the depth from which a signal can be collected.

In addition, the PLPS signal from the underlying α-alumina was collected (Fig. 5b), and plotted against the thickness of the overlaying APS-YSZ coating (Fig. 5d). The signal from

the alumina decays exponentially to zero at a YSZ thickness of ~250 μm. This is consistent with values reported in the literature between 175 μm [35], [40] and [41] and 300 μm [42]. This variation of laser penetration depth in the YSZ layer depends on the microstructure, specifically the distribution and size of scattering sites such as grain boundaries, splat boundaries, cracks and pores in the translucent oxide. The decay of the alumina R2 peak (5023 cm^{-1}) follows Eq. (2) with I_0 = −2.05, A = 105.26 and$B$ = 47.64, whereas for the R1 peak (5053 cm^{-1}) I_0 = −3.01, A = 124.46 and B = 50.84.

4.2. Modelling

Featureless bulk YSZ, with no microstructure, has been used as a control in the modelling to compare with the APS-YSZ and EBPVD-YSZ structures. The computation results are presented in Fig. 6a and b, respectively for an incident laser beam diameter of 1.5 μm. The size of the laser beam diameter at the base of featureless YSZ is 49 μm (FWHM).

The microstructure of APS-YSZ consists of lamellar splats elongated parallel to the substrate (Fig. 1b), and low-refractive index inter-splat boundaries considered to contain air are perpendicular to the incident laser beam (Fig. 7a). Only the large boundaries were considered (Fig. 1a) such that there are approximately five block of splats, each ~50 μm thick and ~80 μm long. The splats were modelled as a material with a refractive index of 2, separated by rectangular air gaps of 50–150 nm. An overview of the ZEMAX computer simulation is shown in Fig. 7b. Fig. 7c and d show the dispersed laser beam diameter and intensity profile results for APS-YSZ, respectively. The beam diameter at the base of the sample is 51 μm (FWHM). Despite significant refraction occurring between the interface at the block boundaries in the APS-YSZ, and hence a large angular deflection (Fig. 7b), the relatively small thickness of the blocks results in very little positional deflection of the laser beam. Thus the change in beam diameter due to the presence of the low refractive index regions in the APS-YSZ is negligible when compared with bulk zirconia.

Fig. 6.

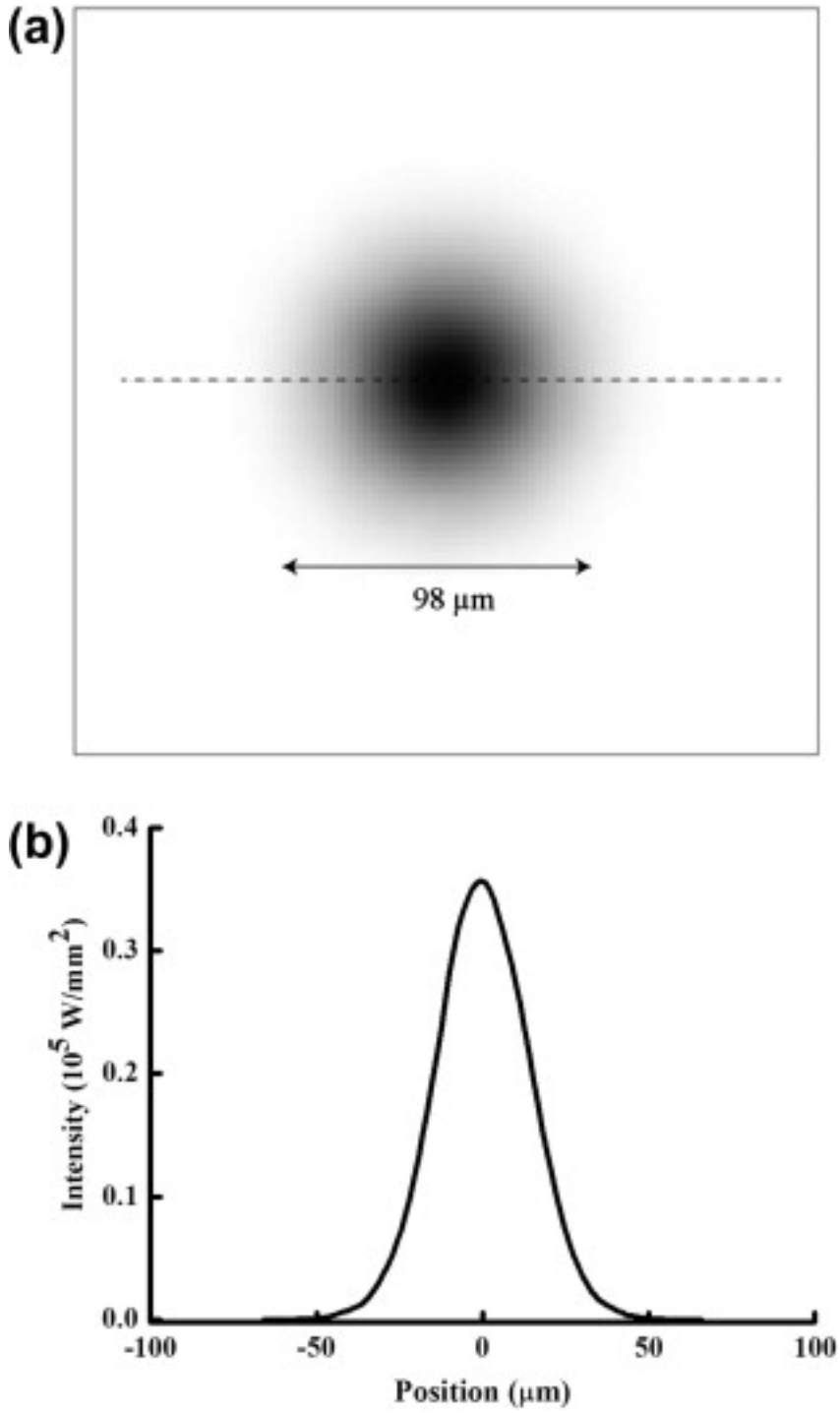

Bulk zirconia reference. (a) Image of irradiance at the base of featureless YSZ, and (b) a cross-section of image (a). When compared to EBPVD-YSZ, the spot diameter at the base is much larger but APS-YSZ has a virtually identical spot size.

Fig. 7.

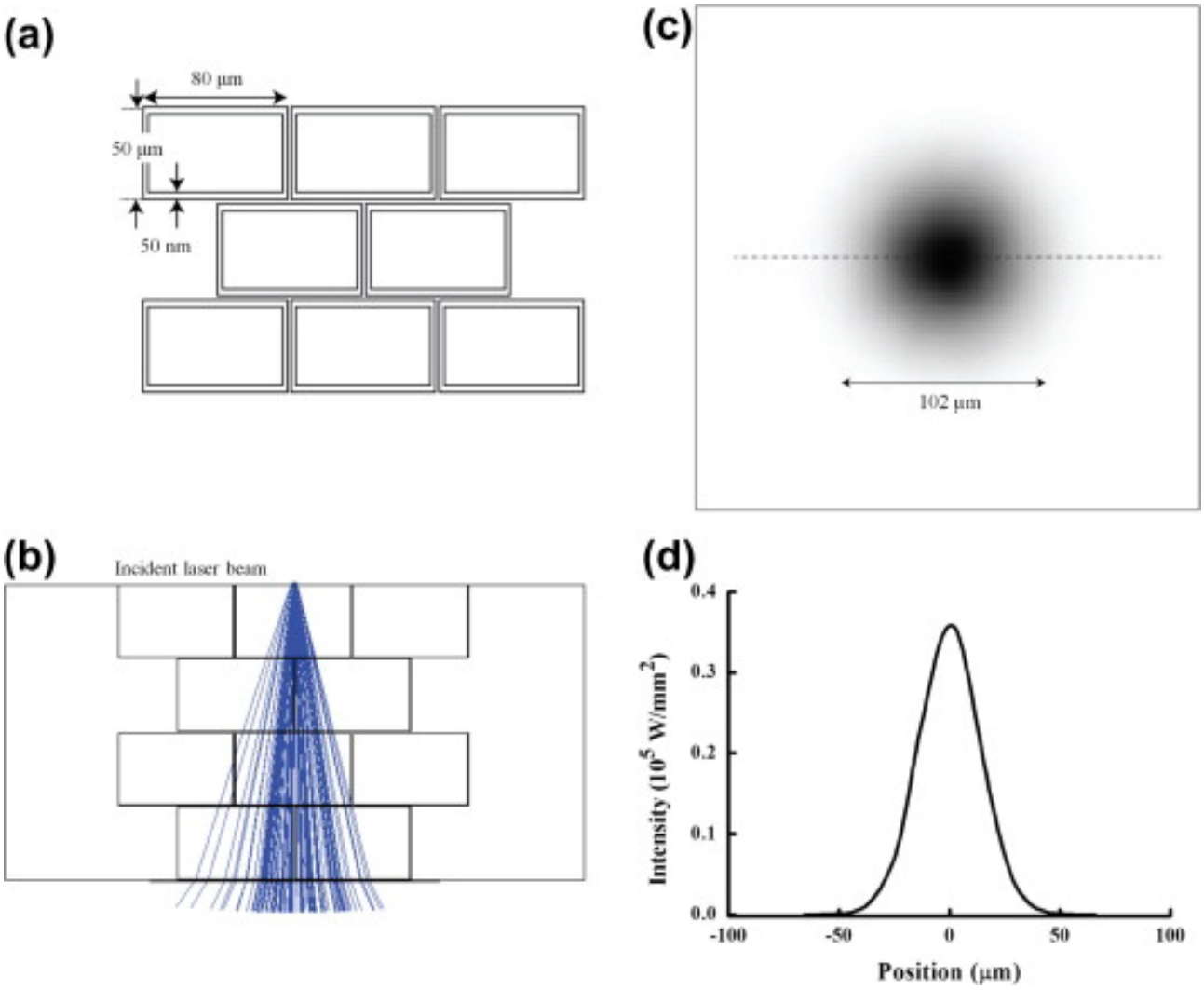

Construction of ray-tracing model of APS-YSZ. (a) Ray-tracing model of APS-YSZ, showing rectangular regions of low refractive index. The thickness of the low-refractive index regions is increased for clarity. (b) ZEMAX ray trace of laser radiation through APS-YSZ. The impact of the low-refractive index regions is minimal. (c) Image of irradiance at the base of YSZ. (d) Cross-section of image (c); FWHM is 50 μm.

The microstructure of the EBPVD-YSZ (Fig. 1b), is approximated by two distinct layers. The top layer (100 μm thick) is an array of trapezoidal columns each separated from its neighbours by a tapered air gap which has a maximum thickness of ~500 nm at the positions of the column tips as shown in Fig. 8a. A layer at the base is ~50 μm thick and consists of columns with an average width of 4 μm separated by an air gap of ~50 nm (Fig. 8b). This simulated structure is shown in Fig. 9a, with the air gaps exaggerated, and in Fig. 9b illuminated by the incident laser beam. An image of intensity distribution produced at the base of EBPVD-YSZ layer is shown in Fig. 9c, and a cross-section in Fig. 9d. The beam diameter is 12 μm (FWHM).

Fig. 8.

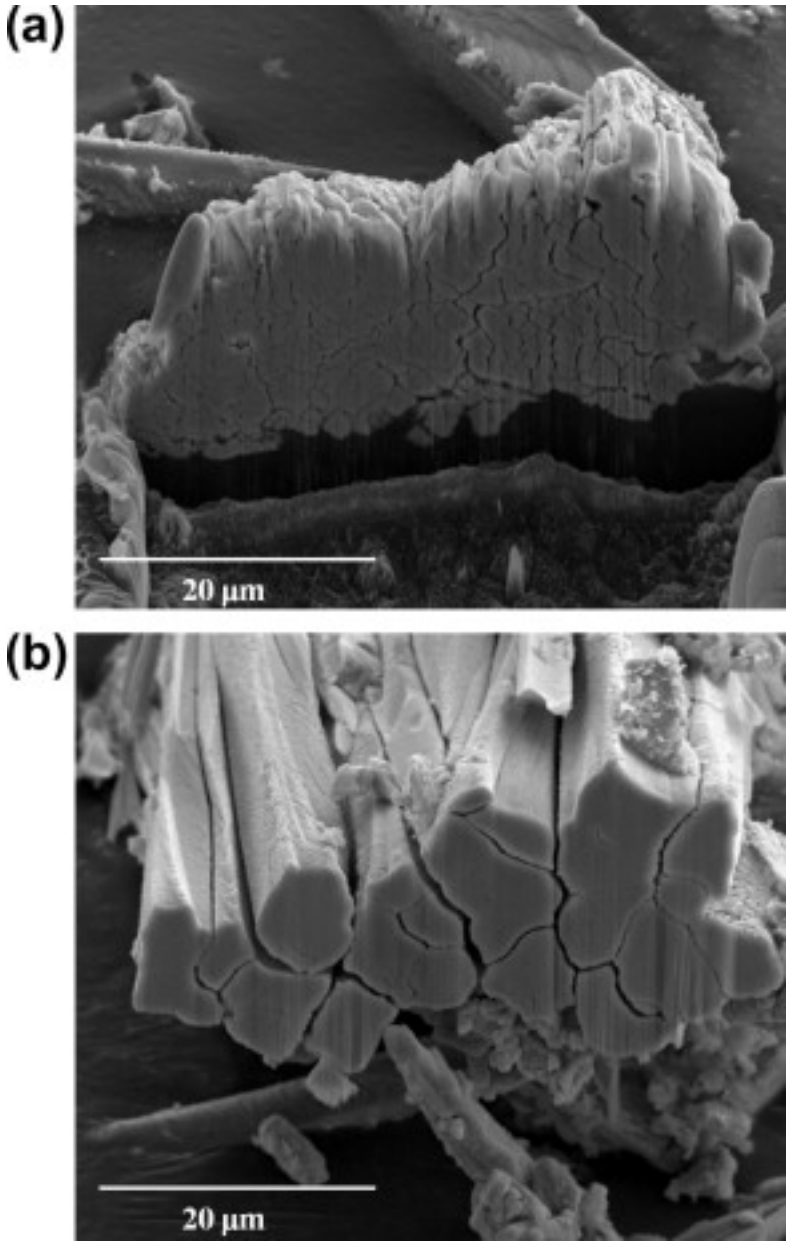

SEM images of cross-sections of a cluster of EBPVD-YSZ showing (a) the root of the columns with small air gaps (~50 nm) and (b) the top of the columns with large air gaps (~500 nm).

Fig. 9.

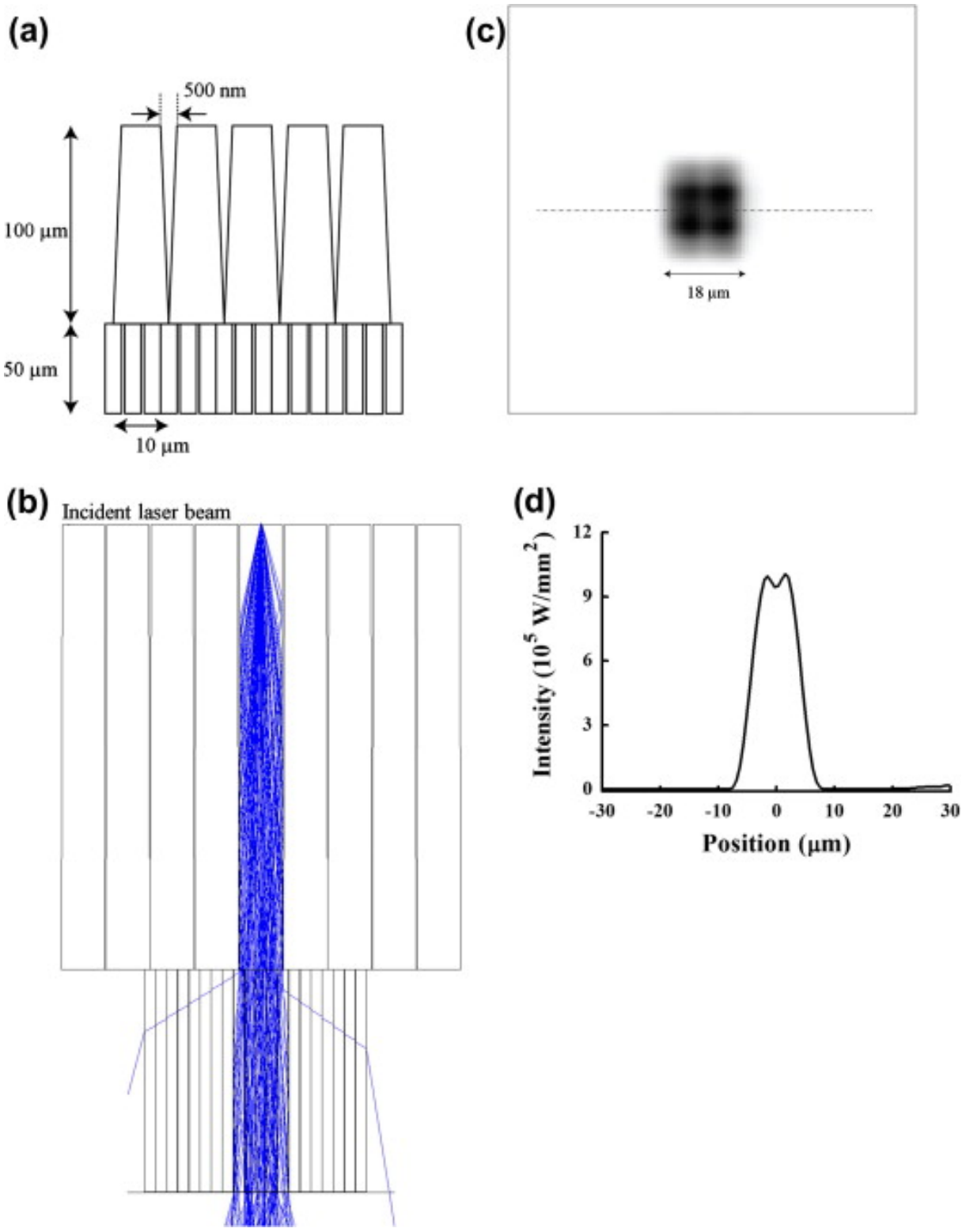

Construction of a ray-tracing model for EBPVD-YSZ. (a) Ray-tracing model structure of EBPVD-YSZ (with air gaps exaggerated) and an image of the observed structure from a sample. (b) Ray-tracing simulation of laser radiation propagating through EBPVD-YSZ; waveguiding limits dispersion and reduces spot size at the root. (c) Image of intensity distribution at the base of YSZ. (d) Cross-section of image (c), limited dispersion results in small spot size (12 µm FWHM).

Zirconia has a high refractive index (~2 for λ = 632.8 nm) compared to the air gaps, and thus the critical angle is low at the interface between the edges of the columns and the air gaps in the EBPVD-YSZ. The low critical angle causes total internal reflection of a large number of rays inside each column, and as a consequence the columns become very effective waveguides for the incident laser beam (Fig. 9b). With each column functioning as a waveguide, the dispersion of the laser radiation is substantially confined to one of the outer large columns, even when the source is placed extremely close to an air gap (Fig. 9c). This results in the very small diameter of the dispersed beam when compared to the APS-YSZ or the control.

5. Discussion

The experimental measurements made for the two commercial TBC materials point to the importance in understanding how the laser beam behaves within the TBC layer when making measurements of stresses, either within this layer or for the embedded TGO that forms at the TBC/BC interface. We will now consider the experimental measurements associated with beam dispersion with respect to several specific factors and also, where appropriate, the predictions for the ray-tracing computer modelling.

5.1. Laser beam dispersion

In the case of experimental tests, the diameter of the laser beam that travels through the EBPVD- and APS-YSZ remained essentially constant after a certain thickness. For the EBPVD-YSZ, this may be because at the thin end of the wedge the microstructure comprises smaller, more densely packed columns (Fig. 8a). Therefore, when the thickness increases the laser diameter increases correspondingly, similar to the exponential trend in dense bulk YSZ. However, when the thickness of the wedge reaches more than 50 μm, the columns with a larger diameter and wider air gaps increasingly contribute to the dispersion of the laser beam. They are the first to disperse the laser beam followed by the denser array of smaller columns at the bottom of the wedge. At this stage, there is a decrease in the increasing rate of the laser beam diameter (Fig. 4). When the thickness reaches ~100 μm, even larger columns come into play (Fig. 8b), which impart little additional dispersion to the laser beam and thus have little effect on its eventual diameter. This is also verified by the modelling (Fig. 9b) which indicates that the change in the dispersion distance along the large columns does not affect the laser beam diameter much but just guides the laser down the columns by internal refraction.

5.2. Comparison of experimental and modelling data

The EBPVD-YSZ computer modelling predicts the intensity distribution at the base of the sample as a square array of four higher-intensity regions related to the four small columns sampled. The square shape in the intensity is due to the simplified square-shaped columns assumed in the model. In practice for the EBPVD-YSZ, the cross-section of each

column has an arbitrary shape with air gaps between (see Fig. 8a and b). The square shape introduced by the model, however, verifies that the dispersion of the laser beam is dominated by the guiding provided by the columns when each ray strikes the sides with an angle smaller than the critical angle. This effect explains why the laser beam dispersion is so much smaller in the EBPVD-YSZ compared to the APS-YSZ.
The APS-YSZ contains randomly distributed pores, intra- and inter-splat defects or boundaries, and foreign dispersion sources such as unmelted zirconia particles and varying yttria concentrations. The model simplifies this complex picture by seeking to consider extracting the most significant lamellar feature of the microstructure. Neglecting the other features such as porosity reduces the degree of dispersion in the model compared with experimental measurements.

The main purpose of the modelling is to help understand the two different dispersion routes within these two different YSZ layers. The channelling of the laser beam within the columns of the EBPVD-YSZ explains why in the case of the experimental measurements the beam is dispersed less in the EBPVD-YSZ than in the APS-YSZ. Therefore, for the same thickness of YSZ layer, the sampling area of the TGO under such an EBPVD-YSZ is smaller than that for an APS-YSZ layer. The model could be improved but it is sufficiently instructive to account for the different responses of the two YSZ materials considered.

5.3. The absorption coefficient of YSZ

Two intensity variations with thickness of the YSZ have been measured: the decay of laser beam intensity through the YSZ layer (both APS and EBPVD), and the decrease in the transmission of the PLPS signal from the alumina layer below the YSZ layer back to the objective lens. The decay trend follow the general form of the Beer–Lambert Law[43]. However, in Eq. (2) the intensities detected in the tested material do not reduce to zero. The optical absorption coefficients ($1/B$) in Eq. (2) gave ~0.010 μm^{-1} (514 and 632.8 nm) for APS-YSZ and ~0.012 μm^{-1} (514 and 632.8 nm) for EBPVD-YSZ, which are of a similar magnitude to those previously determined for dense YSZ (0.05–0.19 μm^{-1})[18] and [43]. In particular, Eldridge et al. [44] and [45] have determined experimentally the scattering and absorption coefficients of freestanding 8 wt.% APS-YSZ (11% porosity) using normal-incidence directional-hemispherical reflectance and transmittance spectra over the range of 250 nm up to 15 μm (data for the range 0.8–15 μm can be found in Refs. [44] and [45]; the range between 250 and 1000 nm is provided by Eldridge and presented in Fig. 10). In Fig. 10, by extracting the values of transmittance for TBCs with different thickness at 514 and 633 nm, an exponential decay can be fitted and the absorption coefficient ($1/B$) is determined to be ~0.01 μm^{-1} for a 514 nm radiation source and 0.007 μm^{-1} for 633 nm. These data are consistent with the values (~0.010 μm^{-1} for 514 and 632.8 nm in APS-YSZ) calculated in this contribution regardless of the potential variations in porosity and microstructure between the two TBCs. Nevertheless, a small reduction in absorption coefficient with the increase in the wavelength of the incident radiation was detected

in Fig. 10, which is not present in our data (see Fig. 3 and Fig. 4). The absorption coefficient of the APS-YSZ samples tested in this paper is smaller than that given by Presser et al. [18] because the sample adopted allows the collection of signals through a thickness of ~250 μm rather than being limited to 40 μm. The difference can be accounted for by the complex microstructure of the two YSZ coatings used in this study which has the potential to reduce the absorption coefficient. The total absorption is proportional to the cross-section of light absorption by a single particle and the density (number per unit volume) of absorbing particles [46]. The smaller value obtained in this set of experiments may indicate that the existence of the pores (15–20% in APS-YSZ [47] and [48]), defects, etc., reduces the density of the equivalent absorptive material.

Fig. 10.

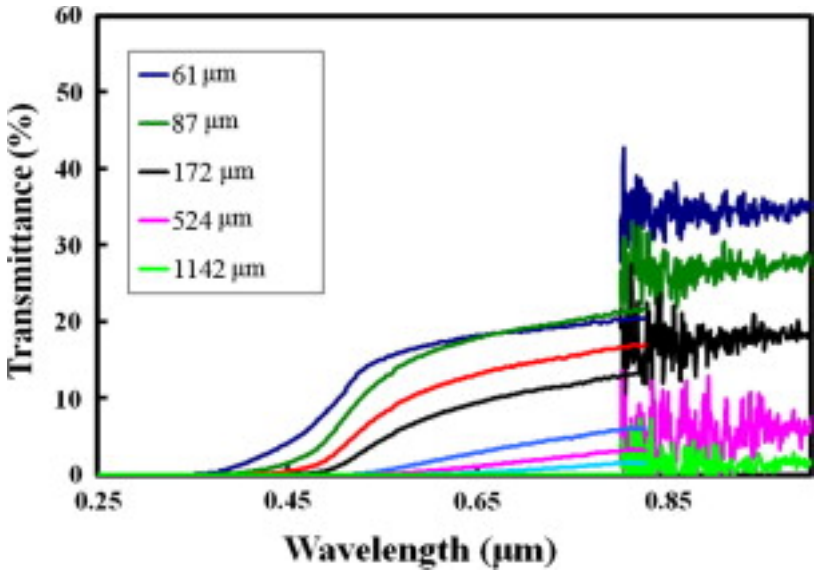

Hemispherical transmittance of freestanding APS-8YSZ measured at room temperature of 23 °C (unreported short-wavelength range room-temperature data from Ref. [45], replotted and presented with the permission from Dr. J.I. Eldridge, NASA Glenn Research Center, USA).

However, for the intensity decay of the alumina PLPS signal, the situation is more complicated. First, the laser light follows a path through the YSZ to reach the TGO and then the emitted fluorescent light has to travel back through the YSZ to reach the detector. This double path length may be responsible for the variation in the absorption coefficient calculated in this case: 0.02 μm^{-1} for the R1 peak and 0.021 μm^{-1} for the R2 peak. It is noteworthy that although the two microstructures (APS-YSZ and EBPVD-YSZ) differ in their degree of lateral beam dispersion, there is little difference in their PLPS absorption coefficients.

5.4. Sampling depth of the Raman spectra in APS-YSZ

A commonly encountered method for measuring the sampling depth of a Raman signal in a material is to create a double-layer system by applying the target material, for example,

a wedge of YSZ, on top of a highly Raman active acryl varnish coating [18]. The intensity decay in the Raman spectra of the acryl varnish is then monitored as a function of thickness. The depth at which the intensity of the Raman spectra emitted from the acryl varnish decreases to zero is defined as the sampling depth. Certainly using this method the laser beam can detect from as deep as 20–50 μm [18], but it does not necessarily follow that the Raman signal excited within the wedge material, YSZ, is from that depth. As demonstrated in this contribution, the laser beam can pass through a thickness of 250 μm of APS-YSZ to excite a Raman signal from the alumina (TGO) but the intensity within the APS-YSZ is limited to a depth of only ~40 μm. Hence the controlling factors are how Raman active the underlying material is and how easy it is for the signal to reach the detector. Therefore, a more reliable way to carry out the commonly used approach is to apply the target material (e.g. YSZ) onto a layer of material with similar Raman activity. Then monitoring the decay of the intensity of the underlying material will provide the sampling depth with higher confidence.

5.5. Technological importance of the sampling volume

For the application of Raman spectroscopy to thermally sprayed YSZ layers, the illuminated volume below the focus of the incident laser beam is cone shaped [46]. The Raman signal collected from the surface extends to about one-fifth of the YSZ layer thickness. The evaluated surface stress derived from a Raman spectra shift is obtained from the volume over which the stress is averaged. Although most of the Raman scattering and the collected signal is from the focus or near-focus region of the incident laser beam, scattering within the out-of-focus region will still contribute to the intensity. There is a gradient of the effective signal across the point of focus on the surface to a depth of ~40 μm as proposed by Presser et al. [18] and 90% of the signal comes from half of the sampled depth.

A reliable measure of beam spreading within the TBC is a prerequisite for mapping of stresses. Two types of non-destructive mapping of residual stresses are often required in TBCs [36], [49] and [50]: mapping of residual stress in the top layer of YSZ and in the underlying TGO. The sampling volume determined in this contribution suggests that for the mapping of the residual stress in APS-YSZ a step interval of ~35 μm should be considered in order to avoid beam overlap and thereby misinterpretation of the evaluated stresses. For stress mapping in the TGO the steps ought to be set as $\geqslant$160 μm for APS-YSZ and $\geqslant$80 μm for EBPVD-YSZ. It is important to make specific measurements of beam dispersion for the specific YSZ coating being addressed.

For other application of Raman spectroscopy, such as the phase detection in materials, the sampling volume is crucial for determining the location and distribution of the detected phases [22] and [23].

6. Conclusions

• The laser diameter increases significantly to 160 μm after dispersion through APS-YSZ with a thickness of 180 μm, compared with ~80 μm for a 120 μm thick layer of EBPVD-YSZ. These results show that the values of 20 μm for APS-YSZ and 100 μm for EBPVD-YSZ previously reported are over-optimistic [51], [52] and [53] for these materials.

• The laser intensity decays exponentially and the absorption coefficient was calculated for the two YSZ materials considered.

• Ray-trace computer modelling for EBPVD- and APS-YSZ coatings revealed that the reduced dispersion in EBPVD-YSZ is a result of the columnar microstructure. Hence the columns act as waveguides which limit dispersion of the incident laser beam.

• The sampling depth of the Raman spectroscopy in APS-YSZ was measured (~40 μm) and compared with an alternative approach reported in literature. Since the results are material dependent, extra care should be taken when making these measurements.

• It is important to take into account the dispersion of the incident laser beam when mapping stresses, particularly for the underlying TGO in TBC systems.

Acknowledgements

We would like to acknowledge the support of The Energy Programme, which is a Research Councils UK cross-council initiative led by EPSRC and contributed to by ESRC, NERC, BBSRC and STFC, and specifically the Supergen initiative (Grants GR/S86334/01 and EP/F029748) and the following companies; Alstom Power Ltd., Doosan Babcock, E.ON, National Physical Laboratory, Praxair Surface Technologies Ltd., QinetiQ, Rolls-Royce plc, RWE npower, Siemens Industrial Turbomachinery Ltd. and Tata Steel, for their valuable contributions to the project. O.T.L. would like to acknowledge support from NERC Grants NE/F019084/1 and NE/H003541/1. Special thanks to Dr. Jeffrey. I. Eldridge (NASA Glenn Research Center, USA) for helpful discussions and providing unpublished data referred to, and included in this paper.

References

[1] Tae KE, Gil YS. Thin Solid Films 1993;227:7.

[2] Fauchais P, Montavon G, Bertrand G. J Therm Spray Technol 2010;19:56.

[3] Evans AG, Mumm DR, Hutchinson JW, Meier GH, Pettit FS. Prog Mater Sci 2001;46:505.

[4] Robert M. Surf Coat Technol A 1987;30:1.

[5] Ahrens M, Vaßen R, Sto¨ver D, Lampenscherf S. J Therm Spray Technol 2004;13:432.

[6] Rickerby DS, Winstone MR. Mater Manuf Process 1992;7:495.

[7] Rickerby DS, Eckold G, Scott KT, Buckley-Golder IM. Thin Solid Films 1987;154:125.

[8] Wu RT, Wang X, Atkinson A. Acta Mater 2010;58:5578.

[9] Tolpygo VK, Clarke DR, Murphy KS. Surf Coat Technol 2004;188– 189:62.

[10] Christensen RJ, Lipkin DM, Clarke DR, Murphy K. Appl Phys Lett 1996;69:3754.

[11] Tomimatsu T, Zhu S, Kagawa Y. Acta Mater 2003;51:2397.

[12] Liu D, Lord O, Flewitt PEJ. Appl. Spectrosc. 2012;66:1204.

[13] Bouvier P, Djurado E, Lucazeau G, Bihan TL. Phys Rev B 2000;62:8731.

[14] Limarga AM, Clarke DR. J Am Ceram Soc 2007;90:1272.

[15] He J, Clarke DR. J Am Ceram Soc 1995;78:1347.

[16] Barberis P, Merle-Mejean T, Quintard P. J Nucl Mater 1997;246:232.

[17] Tanaka M, Hasegawa M, Dericioglu AF, Kagawa Y. Mater Sci Eng

[18] Presser V, Keuper M, Berthold C, Nickel KG. Appl Spectrosc 2009;63:1288.

[19] Nakashima S, Harima H. Phys Status Solidi 1997;162:39.

[20] Hiroshi H. Microelectron Eng 2006;83:126.

[21] Van Manen HJ, Bloemenkamp R, Brink OFVd. Appl Spectrosc 2009;63:378.

[22] Froud CA, Hayward IP, Laven J. Appl Spectrosc 2003;57:1468.

[23] Everall NJ. Appl Spectrosc 2000;54:1515.

[24] Michielsen S. J Appl Polym Sci 2001;81:1662.

[25] Everall N. Appl Spectrosc 2008;62:591.

[26] Baldwin KJ, Batchelder DN. Appl Spectrosc 2001;55:517.

[27] Anderson PS, Wang X, Xiao P. Surf Coat Technol 2004;185: 106.

[28] Lee G, Atkinson A, Selcuk A. Surf Coat Technol 2006;201:3931.

[29] Zhang W, Gan J, Hu Z, Yu W, Li Q, Sun J, et al. Appl Spectrosc 2011;65:522.

[30] Lipkin DM, Clark DR. J Appl Phys 1995;77:1855.

[31] Grabner L. J Appl Phys 1978;49:580.

[32] Ma Q, Clarke DR. J Am Ceram Soc 1993;76:1433.

[33] Ma Q, Clarke DR. Acta Mater 1993;41:1817.

[34] Hough H, Demas J, Williams TO, Wadley HNG. Acta Mater 1995;43:821.

[35] Gell M, Sridharan S, Wen M, Jordan EH. Int J Appl Ceram Technol 2004;1:316.

[36] Wang X, Atkinson A. Mater Sci Eng A – Struct 2007;465:49.

[37] Nychka JA, Clarke DR, Sridharan S, Jordan E, Gell M, Lance MJ, et al. Surf Coat Technol 2003;163:87.

[38] Busso EP, Wright L, Evans HE, McCartney LN, Saunders SRJ, Osgerby S, et al. Acta Mater 2007;55:1491.

[39] Limarga AM, Vassen R, Clarke DR. J Appl Mech – Trans ASME 78:011003.

[40] Sohn Y, Schlichting K, Vaidyanathan K, Gell M, Jordan E. Metall Mater Trans A 2000;31:2388.

[41] Schlichting KW, Vaidyanathan K, Sohn YH, Jordan EH, Gell M, Padture NP. Mater Sci Eng A – Struct 2000;291:68.

[42] Jordan E, Xie L, Gell M, Padture N, Cetegen B, Ozturk A, et al. J Therm Spray Technol 2004;13:57.

[43] Krishna MG, Rao KN, Mohan S. Appl Phys Lett 1990;57:557.

[44] Eldridge JI, Spuckler CM. J Am Ceram Soc 2008;91:1603.

[45] Eldridge JI, Spuckler CM, Markham JR. J Am Ceram Soc 2009;92:2276.

[46] Macdonald AM, Vaughan AS, Wyeth P. J Raman Spectrosc 2005;36:185.

[47] Portinha A, Teixeira V, Carneiro J, Beghi MG, Bottani CE, Franco N, et al. Surf Coat Technol 2004;188:120.

[48] Dombrovsky LA, Tagne HK, Baillis D, Gremillard L. Infrared Phys Technol 2007;51:44.

[49] Wang X, Atkinson A, Chiriv`ı L, Nicholls JR. Surf Coat Technol 2010;204:3851.

[50] Rinaldi C, De Maria L, Mandelli M. J Eng Gas Turb Power 2010;132:114501-1.

[51] Schlichting KW, Padture NP, Jordan EH, Gell M. Mater Sci Eng A – Struct 2003;342:120.

[52] Selcuk A, Atkinson A. Mater Sci Eng A – Struct 2002;335:147.

[53] Rinaldi C, Maria LD, Mandelli M. J Eng Gas Turb Power 2010;132:114501.